Ultrafast X-Ray Diffraction of Heterogeneous Solid Hydrogen

Abe Levitan*
Olin College of Engineering, Needham MA 02492, USA
(Dated: August 19, 2015)

Angularly resolved x-ray diffraction at 5.5 keV establishes the structure of a 5 µm diameter solid hydrogen jet, providing a foundation for analysis of hydrogen in a warm dense matter state. The jet was composed of approximately 65 % ± 5% HCP and 35 % ± 5% FCC by volume with an average crystallite size on the order of hundreds of nanometers. Broadening in the angularly resolved spectrum provided strong evidence for anisotropic strain up to approximately 3 % in the HCP lattice. Finally, we found no evidence for orientational ordering of the crystal domains.

I. INTRODUCTION

Understanding how hydrogen transitions from a crystalline solid to a warm dense matter state is crucial to the success of inertial confinement fusion experiments[1]. Current understanding of the way heterogeneous mixtures of HCP and FCC hydrogen act under compression and heating is limited. To better understand this complex interaction, we captured time-resolved x-ray diffraction spectra from a jet of heterogeneous solid hydrogen undergoing rapid heating. This data will allow us to reconstruct the state of the hydrogen jet as it responds to a rapid influx of energy. Various factors including the crystal structure, the geometry of the crystal domains, and the strain in the lattice affect how the jet absorbs energy.

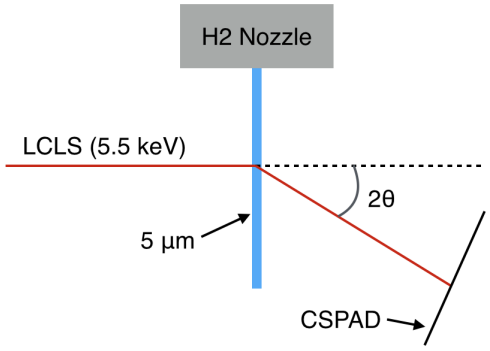

FIG. 1: A diagram of the experimental setup detailing the scattering geometry.

II. EXPERIMENT AND DATA

To understand the structure of the solid hydrogen jet, we analyzed cold angularly resolved X-ray diffraction spectra. 9500 cold spectra were taken, each capturing a single shot of the Linac Coherent Light Source (LCLS) at a photon energy of 5.5 keV and a spotsize of approximately 5 µm (Figure 1). All the spectra were captured directly on on Cornell-SLAC Pixel Array Detectors (CSPADs). An example raw single-shot CSPAD image is in Figure 2, along with the summed image in Figure 3.

The images allow us to build angularly resolved scattering spectra, giving us information about the composition of and strain in the system. They also provide azimuthal information that can be used to pinpoint individual scattering events. By studying the statistics of these individual scattering events we can understand the length scale of the crystal domains.

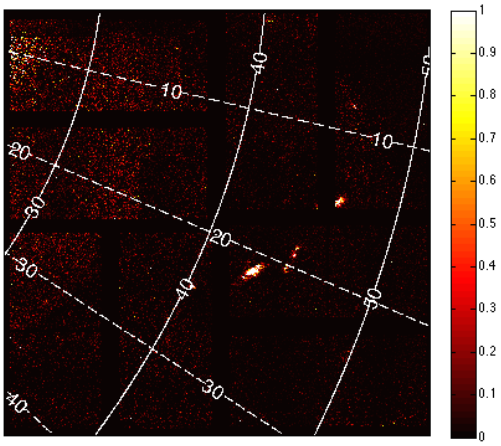

FIG. 2: The raw CSPAD image from a single XFEL shot. Individual scattering events corresponding to single crystallites are easily resolved.

A. Calibration

The CSPAD was calibrated using diffraction data taken from samples with known, sharp scattering peaks. To accurately map pixels to both a polar and azimuthal angle, around 20 calibration points with known scattering angle were manually placed on the image. Then, a model of the laser and sample geometry was fit to the calibration points with a least squares cost function. The fit proved robust to the initial guess and provided an accurate and consistent model of the scattering geometry. Iso-angle lines from the CSPAD calibration are overlaid

* abraham.levitan@students.olin.edu

This material is based upon work supported by the U.S. Department of Energy, Office of Science, Office of Workforce Development for Teachers and Scientists (WDTS) under the Science Undergraduate Laboratory Internship (SULI) program, under Contract No. DE-AC02-76SF00515.

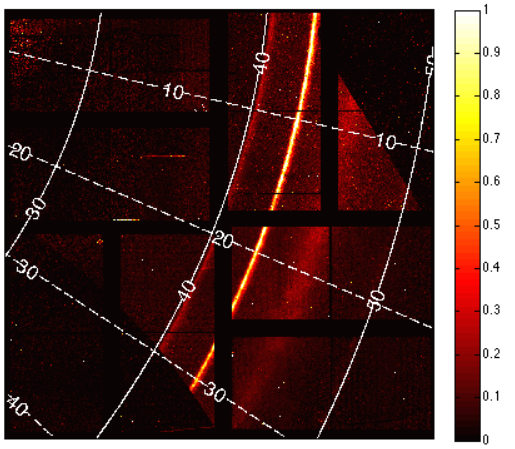

FIG. 3: The raw CSPAD data summed over all 9500 shots. The Debye-Scherrer rings show up clearly in the summed image.

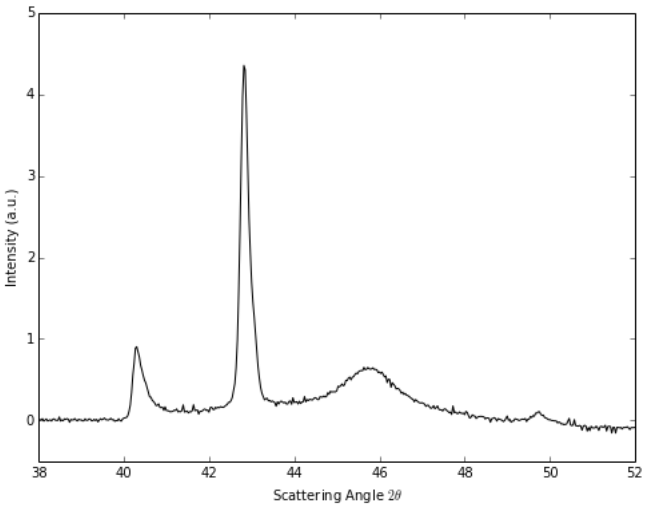

FIG. 4: The summed angular spectrum over all 9500 shots.

on the images in Figures 2 and 3.

Because the scattered x-rays didn't cover the entire detector, we manually masked off the dark top-left and bottom-right regions of the detector (seen clearly in Figure 3). All histograms were generated by binning unmasked pixels according to polar or azimuthal angle and computing the mean intensity within each bin. Only sampling from areas of the CSPAD that contained real data prevented "dark" pixels on the detector from artificially dragging down the intensity readings.

III. ANALYSIS

A. Crystal Structures

The volume fraction of HCP and FCC in the jet was calculated using the summed spectrum over 9500 shots (Figure 4). We compared the integrated intensities under the first two scattering peaks with calculated powder diffraction intensities of HCP and FCC hydrogen (Figure 5). The relationship is defined by:

$$\frac{\text{peak 1}}{\text{peak 2}} = \frac{\{010\}_{\text{HCP}}}{\{002\}_{\text{HCP}} + \{111\}_{\text{FCC}}} \tag{1}$$

We calculated the expected peak intensities by approximating the form factor of molecular hydrogen as a doubling of the form factor of atomic hydrogen. A comparison with real scattering data from HCP hydrogen[2] indicated that using this form factor produces accurate spectra. Using this approximation, the peak ratio $\frac{\text{peak 1}}{\text{peak 2}}$ of 0.28 in the scattering spectrum corresponded through Equation 1 to a volume fraction of 65 % HCP.

There is a subtle source of error that can enter this calculation, however. If the distribution of the HCP phase is not uniform in the jet, higher fluence areas nearer to the laser spot would contribute more to the scattering intensity, possibly allowing more or less HCP to show up in the scattering data than the true volume fraction.

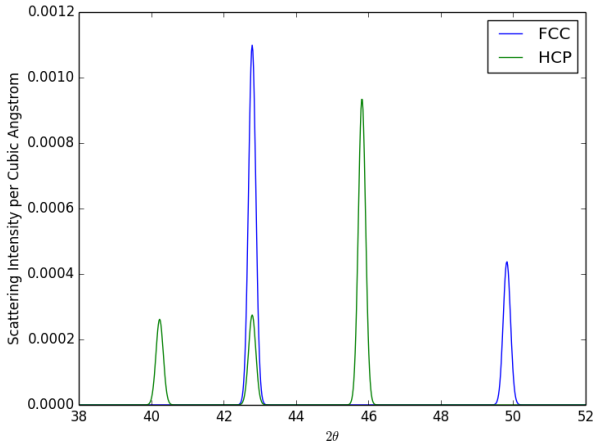

FIG. 5: Calculated FCC and HCP spectra for a 50:50 mixture. The calculated peak intensities are used to derive the HCP volume fraction in the hydrogen jet.

We assessed the amount of error that such distributions could introduce with a simple geometric model of the interaction region. We had focused the LCLS spot to a 5 µm FWHM profile and were probing a 5 µm beam diameter. For this particular system, the effect of the non-uniform distribution is limited to a few percent (Figure 6).

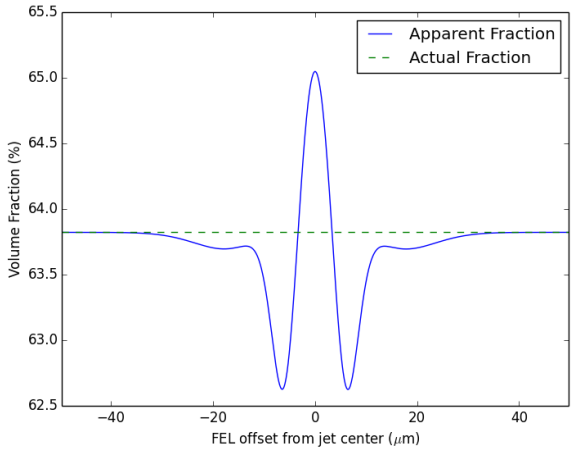

FIG. 6: Simulation of a 10 µm FWHM laser spot interacting with a 5 µm jet. This jet is a purely FCC sheath surrounding a purely HCP core, exaggerating the effect of the laser-jet offset. The maximum variation is 1.5 %.

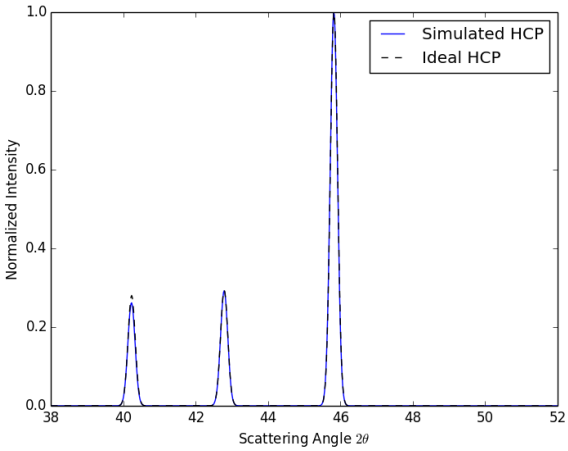

FIG. 7: Comparison of the calculated scattering spectrum for HCP Hydrogen to a spectrum produced by a monte carlo simulation of 100,000 crystallites.

B. Crystallite Sizes

Information on crystallite size usually comes from two disparate sources. First, small crystallites create a noticeable broadening in the scattering peaks due to the finite size of the crystal domain. If this is the only major source of peak broadening, it can be used to accurately calculate the size of crystallites in the material using the Scherrer equation[3]:

$$\tau = \frac{K\lambda}{\beta \cos(\theta)} \tag{2}$$

This relates the crystallite length τ to the shape factor $K \approx 0.9$, the x-ray wavelength λ, the peak broadening β, and the scattering angle θ.

Equation (2) indicates a crystal size on the order of tens to hundreds of nanometers. This is inconsistent with the scattering statistics in our experiment - a system with any significant volume fraction of 10 nm crystals would contain many more scattering events per shot than were actually recorded. Thus, we believe that the strain gradient in the crystals dominated the broadening in the scattering peaks.

We can also calculate the crystallite size using the shot-by-shot scattering statistics. With the geometry and beam fluence profile, we can relate the scattering statistics to the particle sizes.

We used a Monte Carlo simulation to investigate both of these effects. Our simulation directly simulates x-ray diffraction from a finite number of randomly oriented crystal domains, assuming a uniform distribution of phases with a 65 % HCP volume fraction. Scattering intensity is calculated from each reciprocal lattice vector assuming a finite "capture region" inversely proportional to the crystallite size where scattering is allowed. The "capture region" approximation was significantly less computationally intensive than the full expression for intensity variation and able to well approximate the Scherrer formula (2) for peak broadening.

Simulated scattering spectra with hundreds of thousands of crystallites consistently matched calculated powder diffraction spectra in the infinite crystallite limit (Figure 7). This provided evidence that the capture region approximation preserved the correct statistics for crystallite alignment. Finally, the predicted absolute scattering intensities were consistent across a range of crystallite sizes (Figure 8), indicating that our scaling laws for crystal size were correct.

Finally, the simulation also accounted for the geometry of the interaction region. For each shot, the simulation separated the interaction region into 100 sections by beam fluence. Thus, the effect of lower fluence parts of the beam hitting more jet area is naturally included in the simulation.

However, too little was known about the system to be able to place confidence in the Monte Carlo simulation's results. The predictions depended strongly on the profile of the beam and the geometry of the jet, the distribution of crystallite sizes, and the sensitivity of the detector. While the simulations strongly point to a crystallite size in the hundreds of nanometer range, further accuracy is unfeasible until more aspects of the experimental system are characterized.

C. Lattice Strain

We developed a simple nearest-neighbor model of the hydrogen HCP lattice to find the lowest-energy eigen-

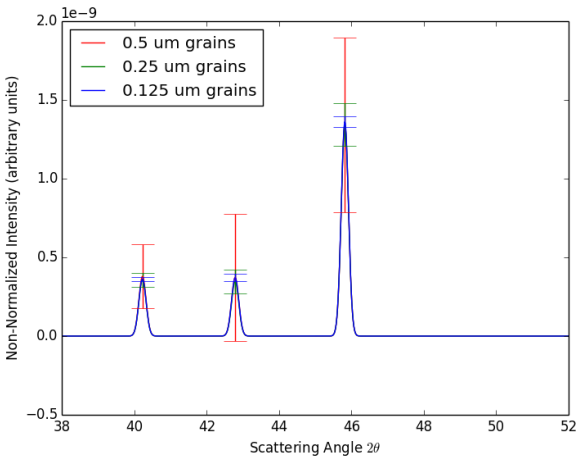

FIG. 8: Comparison of simulated scattering spectra for HCP. Each spectrum is averaged over 100 shots - the mean spectra remain the same, while uncertainties increase with crystallite size.

modes of strain. The model assumed a purely radial potential with a quadratic energy well - reasonable assumptions for small deformations, given that the hydrogen solid is held together by Van Der Walls forces and pushed apart by degeneracy pressure[4]. The actual depth of the quadratic well doesn't matter for our analysis, as we only need to rank the strain modes (we don't need to know the actual stress-strain relationship).

We used the simple model to write a function for the potential energy U as a function of the strain tensor $\boldsymbol{\epsilon}$. We then expanded $U(\boldsymbol{\epsilon})$ in a Taylor series about $\boldsymbol{\epsilon} = \mathbf{0}$, corresponding to no strain.

$$U(\boldsymbol{\epsilon}) \approx U_0 + \left[\frac{\partial U}{\partial \boldsymbol{\epsilon}}(\boldsymbol{I})\right]_{\alpha\beta} \boldsymbol{\epsilon}^{\alpha\beta} + \frac{1}{2}\left[\frac{\partial^2 U}{\partial \boldsymbol{\epsilon}^2}(\boldsymbol{I})\right]_{\alpha\beta\gamma\delta} \boldsymbol{\epsilon}^{\alpha\beta}\boldsymbol{\epsilon}^{\gamma\delta} \tag{3}$$

The first order term $\frac{\partial U}{\partial \boldsymbol{\epsilon}}$ is necessarily 0 because we are considering an equilibrium state. By considering the eigentensors and eigenvalues of the second order term $\frac{\partial^2 U}{\partial \boldsymbol{\epsilon}^2}(\boldsymbol{I})$ we can pinpoint the lowest energy strain modes. The two lowest energy modes (which share an eigenvalue) are pictured in Figure 9.

The low energy eigenmodes of strain are shearings of the lattice in the plane perpendicular to the c-axis. These strain modes in real space correspond to shearings of the reciprocal lattice. At low deformations, they preserve the length of the reciprocal lattice vectors in the {010} and {002} families. However, this shearing distinctly alters the length of the vectors in the {011} family. This family contains 12 distinct scattering vectors, each of which is in general oriented differently with respect to the shear. Thus, the effect of these strain eigenmodes is to maintain the sharpness of the {010} and {002} peaks, but quickly spread the {011} peak. Example spectra showing this

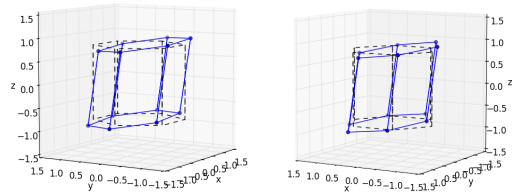

(a) Mode 1 (b) Mode 2

FIG. 9: Visualization of the two lowest-energy strain modes. They correspond to two different shearings of the HCP lattice.

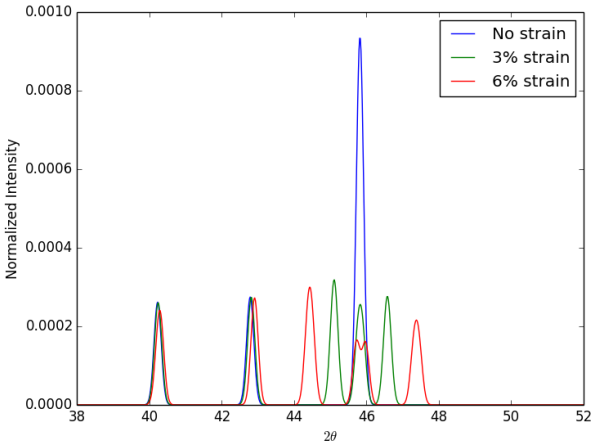

FIG. 10: Several spectra generated with different strain tensors from a Mode 2 deformation.

effect are shown in Figure 10

We can make a quantitative prediction by generating powder diffraction spectra averaged over many linear combinations of low energy eigenmodes. We generated scattering spectra by assuming a gaussian distribution of strain with an equal distribution of strain between the two low energy modes. The associated strain for each spectrum is the standard deviation of that gaussian. By comparing the simulated spectra to the actual spectrum (Figure 11), we can estimate the strain to be on the order of 3%.

D. Crystallite Orientations

Due to the asymmetry of the hydrogen jet itself and the asymmetry of the cooling process, it seems likely that there could be preferred directions of crystal growth. Any preferred direction of growth would show up in the scattering spectra as a dependence of the scattering intensity on azimuthal angle. However, we see no azimuthal variations in the {010} or {002} peaks.

The azimuthal scattering data from the {011} peak

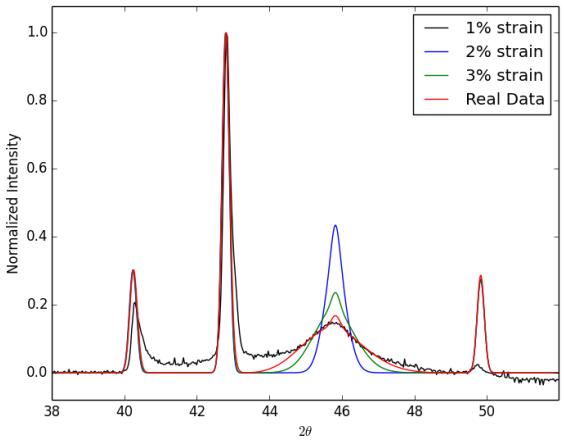

FIG. 11: Comparison of simulated spectra averaged over low energy eigenmodes of strain to the measured scattering spectrum.

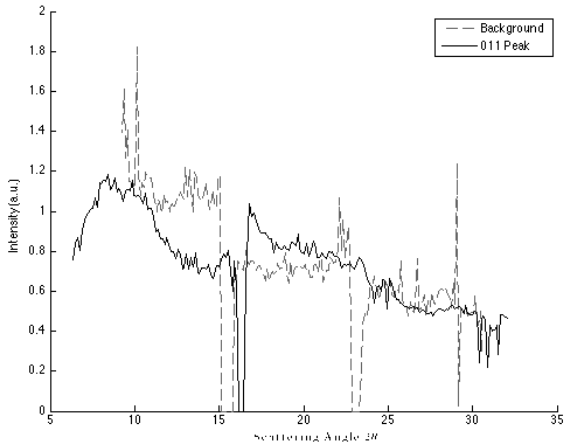

FIG. 12: The azimuthal variation in the {011} peak's intensity. It is correlated strongly with the background noise level on each tile of the CSPAD. The variation from 5° to 15° is due to the {011} peak only grazing the tile sampled in the background.

does contain significant variation with azimuthal angle (Figure 12). However, this variation is due to a difference in sensitivity between neighboring tiles on the CSPAD. We believe that the calibration of the CSPAD tiles was done incorrectly.

We cannot completely rule out the presence of orientational ordering. This is because the azimuthal angles at which we expect to see peaks in scattering intensity all lie out of the detector's range. A further experiment with a small change in the CSPAD location could easily provide definitive evidence for or against crystallite ordering.

IV. CONCLUSION

The cold x-ray diffraction spectra reveal the low-temperature structure of the hydrogen jet. Using these data, we determined key jet parameters — the HCP volume fraction and the approximate crystallite size scale — and we identified significant strain in the HCP phase.

The unexpectedly weak scattering from the {200} FCC lattice planes remains unexplained. A more accurate calculation of the scattering form factor for molecular hydrogen could account for the difference. Additionally, crystallite ordering could be significantly affecting the calculated HCP volume fraction and increasing the expected intensity of the peak.

Despite the remaining puzzles, the data so far paint a clear picture. The jet contains a heterogeneous mixture of HCP and FCC crystals with a moderate HCP majority. The HCP crystals experience a large amount of anisotropic strain, in contrast to the FCC crystals. Finally, the crystals domains are on the order of hundreds of nanometers wide, and do not appear to be ordered in any significant way.

ACKNOWLEDGMENTS

I am grateful to Luke Fletcher and Michael MacDonald for coming up with the idea to give me this project, as well as for mentoring me through it. Additionally, I want to thank the United States Department of Energy for funding the SULI program, and Enrique Cuellar for doing an amazing job of running the SULI program at SLAC.

[1] S. H. Glenzer *et al.*, Physics of Plasmas **19**, 056318 (2012).
[2] H.-K. Mao, A. Jephcoat, R. Hemley, L. Finger, C. Zha, R. Hazen, and D. Cox, Science **239**, 1131 (1988).
[3] R. Jenkins and R. L. Snyder, *Introduction to X-ray Powder Diffractometry* (John Wiley & Sons, Inc., 1996) p. 90.
[4] F. Königsmann, *Femtosecond spectroscopy of solid hydrogen: Long lived coherences in a molecular quantum crystal*, Ph.D. thesis, Freien Universität Berlin (2012).